

Impact of Ground Effect on Circulation Controlled Cylindrical Surfaces

Byron W. Patterson

*West Virginia University (WVU)
Mechanical and Aerospace Engineering Dept. (MAE)
Center for Industrial Research Applications (CIRA)
PO Box 6106
Morgantown, West Virginia, 26506, USA*

bpatter6@mix.wvu.edu

Gerald M. Angle, II

*West Virginia University (WVU)
Mechanical and Aerospace Engineering Dept. (MAE)
Center for Industrial Research Applications (CIRA)
PO Box 6106
Morgantown, West Virginia, 26506, USA*

Gerald.Angle@mail.wvu.edu

Emily D. Pertl

*West Virginia University (WVU)
Mechanical and Aerospace Engineering Dept. (MAE)
Center for Industrial Research Applications (CIRA)
PO Box 6106
Morgantown, West Virginia, 26506, USA*

Emily.Pertl@mail.wvu.edu

James E. Smith

*West Virginia University (WVU)
Mechanical and Aerospace Engineering Dept. (MAE)
Center for Industrial Research Applications (CIRA)
PO Box 6106
Morgantown, West Virginia, 26506, USA*

James.Smith@mail.wvu.edu

Abstract

Circulation control technology and motion in close proximity to the ground have both shown aerodynamic benefits in the generation of lift. Recent research efforts at West Virginia University have explored the potential of merging the two phenomena, in an attempt to enhance both technologies. This paper initiates this combined effort by experimentally investigating the impact ground effect has on the separation location of a jet blown tangentially over circulation controlled cylindrical surfaces. Previous experimental research on circulation controlled cylinders found an optimal radius of curvature and volumetric flow rate; whose model and optimal findings are built upon by this work through the addition of ground effect analysis by varying the ground height. The experiment investigates some of the variables that individually influence circulation control and ground effect; the variables are the radius of curvature, velocity of the jet, and the height from the ground. Data analysis revealed that for a constant volumetric flow rate and varying the height to radius (h/r) value, there is a large amount of variability in the data, indicating that the proximity of the ground has significant impact on the separation location and consequently influence on the potential lift characteristics. Furthermore, when this flow rate was analyzed, it was found that at an h/r of approximately 4.8, it appears that an optimal h/r occurs, based on the surface pressure and flow separation from the cylinders when not influenced by the ground. The data also found that at both radii, 0.520 and 0.659 inches, showed benefit when tested in close proximity to the ground. The findings demonstrate that there is further enhancement potential of the lift generating capability by uniting the lift enhancement of circulation control methodology with the ground effect flight regime.

This effort is a preliminary study of a larger effort to determine if merging the two phenomena indicates a lift enhancement. This model does not have a free stream velocity, and subsequently does not measure

lift, however, the findings depicted in this effort indicate that there is potential for enhancement, which is currently being researched by the authors.

Keywords: Ground Effect, Cylindrical Jet, Jet Separation

1 INTRODUCTION

This research effort combines the aerodynamic benefits of circulation control technology along with the added benefits of typically associated with ground effect flight. Circulation control is a lift augmentation technology that improves the coefficient of lift of a conventionally shaped lifting surface. A circulation control wing differs from the traditional wing largely in the trailing edge. A circulation control trailing edge is normally blunt and circular, whereas the conventional wing has a sharp edge. While there is an additional amount of lift generated by a circulation control surface, the trailing edge tends to increase the effects of parasitic drag [1]. Along with an altered trailing edge, other geometric differences of the circulation control wing include the presence of air chambers within the structure, and the jet slots used to supply the energized jet to the rounded trailing edge.

Circulation control technology has been applied to a wide range of applications, including Short Take-off and Vertical Landing (STOVL) vehicles. It is a desired method for STOVL applications since these vehicles are designed for remote locations, where a normal length runway is not available. The high lift benefits provided by a circulation control wing allow the vehicle to land in little to no space due to the lower horizontal speed requirements to obtain a specific lift force. Besides STOVL vehicles, circulation control has been adapted for use on helicopter rotor blades, wind turbines, watercraft, and ground effect and ground contact vehicles.

The second phenomena considered in this investigation is the benefit gained through ground effect motion. Similar to circulation control, the presence of a lifting surface induced by ground effect results in larger lift coefficients. This result can simply be explained by realizing that as a lifting surface approaches the ground the air underneath the wing becomes pressurized, similar to a ram pressure. Thusly, as the air pressure increases, an increase in the lift created by the surface is noticed. Traditionally, ram pressure describes a technique that forces air underneath the lifting surface, however, for this effort, the term is used to describe the increased pressure due to flow onset.

Many efforts have been conducted on trying to design the structure of the lifting surface so as to capture more of the ram pressure effect, thereby increasing the overall lift. Mantle presents a multitude of designs for aerodynamic cushion craft forms, which have a downward shaped structure at the furthest outboard location of the wing; some of wings are called ram wings and channel flow wings, illustrating the focus of ram pressure on a wing in ground effect [2]. While the wings presented by Mantle are altered to capture the ram pressure and increase the lift, traditional wings also experience ground effect; however energy is often lost from the pressure gradient at the wing tips [2]. Just as with circulation control, inducing the phenomenon of ground effect has been applied to many applications including STOVL vehicles, hovercraft, and watercraft. While both of the presented phenomena have benefits by themselves, amalgamating the two potentially permits further lift and possibly control benefits, applicable for many industries including wind turbines, motorsports, and automotive.

This research effort explores the merging of the two phenomena, attempting to determine whether the combination further enhances or detracts from each other. To investigate the influences of the two lift enhancements, a model was constructed that identifies the angular separation point of a blown jet on a cylinder, which represented the trailing edge of a circulation control airfoil, with decreasing height above a ground plane. Since the model does not have any free stream velocity, the ram pressure as explained is not considered at this point in the research program, since this effort is a preliminary study in order to determine if further wind tunnel research where flow onset is present is needed. Rather, the surface pressure on the cylinder is measured as a function of the angular location from the slot exit. The data from the angular surface pressure can then be compared to the same quantity but at a different height above the ground. What's more, the performance of a ground effect induced circulation control cylinder is

now believed to be dependent upon a multitude of variables including, but not limited to, the trailing edge radius, the velocity of the jet, and the height from the ground.

2 BACKGROUND

2.1 Circulation Control

Circulation control technology exploits a fluid dynamic phenomenon, known as the Coanda effect. This phenomenon, discovered by Henri Coanda in 1910, is experienced by the common person on a daily basis [3]. A simple example is when a liquid is poured from a glass, the liquid has a tendency to adhere to the edge and curl around, resulting in the annoying dribble of liquid from the glass. Another example is when a finger is placed, or the back of a spoon, under a thin water stream from a faucet, the stream attaches to the finger, flows around the blunt object, and again becomes a uniform flow on the adjacent side. It is necessary to point out, that for the latter example, while the flow is uniform on the adjacent side, the flow is at an angle offset from the original direction; this concept can be applied to circulation control lifting surfaces, where the finger is represented by the circular trailing edge of the modified airfoil, and the flow is shown by the energized air in the model produced by the jet slots. Reba [3] defines the anomaly as the tendency of a fluid, either gaseous or liquid, to cling to a surface, that is near an orifice from which the fluid emerges. Newman [4] offers an alternate definition, describing the Coanda effect as the deflection of plane jets by adjacent boundaries.

Similar to the glass of liquid and stream of water visuals, the Coanda effect can be experienced on a circulation control surface. The air flowing over a lifting surface can be influenced by a jet of air blown out of a small slot over a region of a surface. Some of the research efforts have utilized a circulation control lifting surface with two orifices for the jet of air to expel, which are located at the top and bottom of the circular trailing edge, shown in FIGURE 1. This dual slot configuration enables the ability to increase or decrease the lift force generated, together or alternately if required. Along with the exit slot difference, a circulation control wing or lifting surface differs from the conventional wing by the blunt trailing edge and the internal plenum structure for the energized air supply, shown by the NASA 0417 airfoil and the NASA 0417 CC airfoil. Many efforts, however, including this work, utilize only one exit slot, illustrated in FIGURE 2.

The Coanda effect would not be as advantageous for the standard airfoil design, such as the NASA 0417 airfoil with a sharp trailing edge. If a blown jet were applied to this conventional design, the fluid would adhere to the surface until the sharp point, where the flow would break from the airfoil, consistent with the Kutta condition. This would result in a jet flap, which produces beneficial lift performance, however, this enhancement is met by a higher energy cost in the pumping of the air than a circulation control airfoil like the NASA 0417 CC airfoil with the rounded trailing edge.

As the fluid leaves the slot, b , in FIGURE 2, whether with one or two orifices, the jet, at a given jet velocity, V_{jet} , attaches to the surface due to the imbalance of centrifugal and pressure based suction (vacuum) forces [3]. This effort uses the term 'vacuum' to describe the pressure gradient of the energized jet. As observed by Henri Coanda in his jet exhaust efforts, due to the presence of an increased jet velocity, the pressure on the surface of the cylinder is less than the atmospheric pressure, creating a vacuum that pulls the jet towards the surface [3]. As the air traverses an angular displacement, θ , along the cylinder, the air reaches the separation point, where the free stream pressure, p_∞ , and the pressure at the surface are equalized by the inertia (centrifugal) force of the jet, culminating in a zero net force, and the separation of the flow from the cylindrical edge. Newman found by theoretical calculations that the fluid has the potential of attaching through angular displacement of up to 180 degrees from the jet exit [4].

Previous efforts by the authors have found empirically that with an optimal radius of curvature and jet velocity, the energized air has the potential to attach at angles up to 231 degrees [5]. In addition, this jet has a higher velocity than the surrounding free stream air, resulting in a pressure gradient that pulls more air into the low pressure segment called entrainment. The further entrainment of air into the flow increases the angular displacement of the boundary layer, and increases the amount of the jet attached to the surface. Coanda found that as the jet flowed around the edge, it entrained up to 20 times the amount of air, relative to the original jet [3].

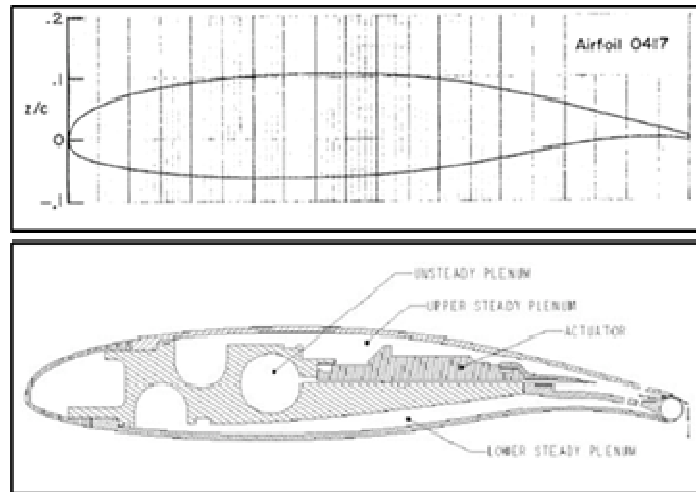


FIGURE 1: NASA 0417 airfoil (above) [6] and NASA 0417 CC airfoil (below) [7]

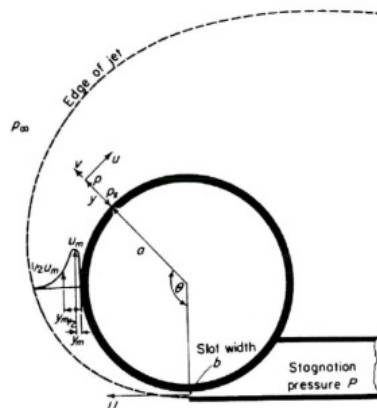


FIGURE 2 : Fluid flow around a cylinder [4]

The main advantage of circulation control technology over traditionally shaped lifting surfaces is the increase in lift due to the attachment of the energized air flow. Fisher [8] found that a circular cylinder consistently produced greater Lift-to-Drag (L/D) values than the 50% ellipse airfoil, whose results were found to be comparable to a conventional airfoil. His findings indicate that the drag on the circular cylinder was minimized as the lift was optimized, showing that when the blown jet is activated, the circulation control model's drag was overcome by a larger increase in lift. Fisher also found that a circulation control airfoil outperformed the 50% ellipse airfoil, in regards to the L/D value. Note that this result is only applicable during periods of jet activation [8]. Along with the findings of Fisher, Cagle and Jones found that as the velocity of the jet of air increases, there is an increase in the coefficient of lift, as shown in

FIGURE 3 [7]. In Cagle and Jones' graph, the velocity of the jet is non-dimensionalized through the blowing coefficient, C_{μ} , which relates the slot height t , the chord length c , the ratio of specific heat γ , the ambient density ρ_{∞} , the free stream velocity V_{∞} , the Mach number of the air jet at the slot M_j , and the plenum pressure P_o , as defined by Ambrosiani in Eq. (1) [9].

Englar [10] offers an alternate definition of the blowing coefficient per unit span in Eq. (2), which is dependent on the mass flow rate \dot{m} , velocity of the jet V_j , the dynamic pressure q and the chord length c [10]. Cagle and Jones' findings show that for $C_{\mu} = 0$ and $C_{\mu} = 0.060$, there is a lift enhancement of around 2.5, corresponding to a maximum coefficient of lift of 1.3 and 3.4, respectively. A traditional NASA 0417 airfoil is proven to generate a maximum lift coefficient of 1.8 [6]. Thus, when a circulation control airfoil is compared to a traditional airfoil, there is a lift generation by a factor of around 2.

$$C_{\mu} = \frac{t}{c} \frac{2\gamma M_j^2}{\rho_{\infty} V_{\infty}^2} P_o \left[1 + \frac{\gamma - 1}{2} M_j^2 \right]^{\frac{-\gamma}{\gamma - 1}} \quad (1)$$

$$C_{\mu} = \frac{\dot{m} V_j}{q c} \quad (2)$$

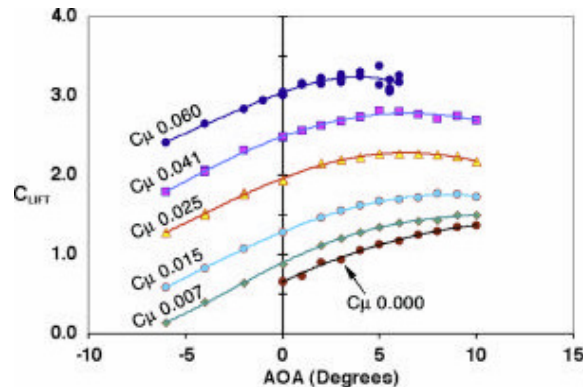


FIGURE 3 : NASA CC 0417 C_L [7]

However, along with large amounts of lift, the geometry of a circulation control airfoil in FIGURE 1 generates a substantial amount of parasitic drag, during periods of deactivation, due to the altered trailing edge shape. When comparing a conventional NACA 0018 airfoil and a NACA 0018 circulation controlled airfoil at a similar Reynolds number of 4.0×10^5 , and coefficient of lift of 0.60, the coefficient of drag was 0.018 and 0.763, respectively [11]. The data for the circulation control NACA 0018 was collected by one of the authors for a CC-NACA0018 wind turbine project [12].

The origin of this effort stems from a previous effort by the authors to explore the relationship between the radius of curvature, jet velocity, and angular separation [5]. The results are shown in FIGURE 4. As the radius of curvature increased, there was a decrease in the angular separation point. Conversely, as the jet velocity increased, there was a delay in the separation of the flow, increasing the angle from the jet exit to the point of separation. This effort culminated in an optimal cylinder radius and jet velocity, as related to the separation point, resulting in a radius of 0.659 inch and a volumetric flow rate of $30 \text{ ft}^3/\text{min}$. For this current research effort, the optimal radius was used, along with the 0.52 and 0.943 inch radius cylinders, which were the closest to the optimal radius of those previously tested.

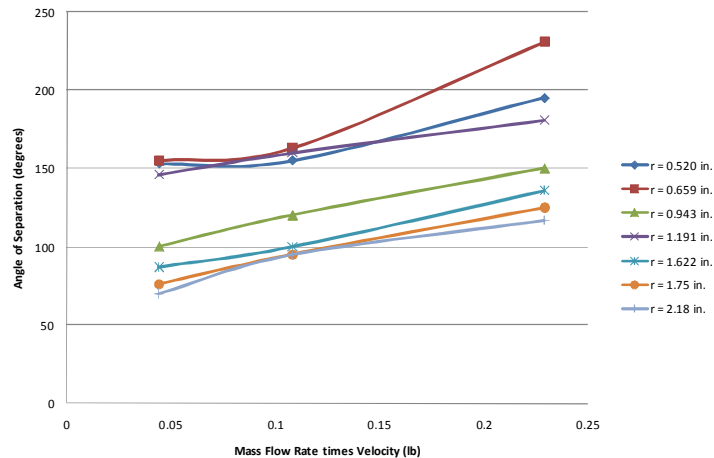


FIGURE 4 : Angle of separation and mass flow rate velocity [5]

2.2 Ground Effect

The second phenomena that this effort considered was the additional lift experienced while a moving surface is in ground effect. Mantle defines an air cushion craft as “any craft designed to operate for a significant periods of time in the proximity of the surface over which it operates and to generate a significant part of its lift through pressurized airflow” [2]. Mantle later states in his introduction that his definition also applies to the ram wing, wing in ground effect, WIG, and channel flow craft. Both the ram wing and the channel flow craft were described in the introduction section of this paper. The previous definition is illustrated in FIGURE 5, showing how the air pressure generates under the craft and influences the surroundings. Mantle documents two performance gains by flying in ground effect. The first performance gain is that the stagnation point, defined by the Kutta condition, at the rear of a wing moves aft on the under surface. This movement increases the curvature of the streamlines, resulting in an increased circulation and lift. The second performance gain results because, as the wing approaches the ground, the span wise flow to the tip is lessened, weakening the tip vortices, and decreasing the lift induced drag [2].

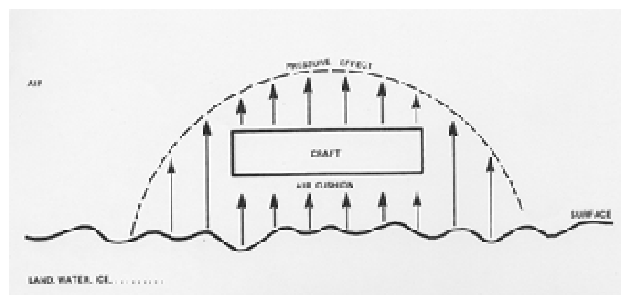


FIGURE 5 : Air cushion craft [2]

The coefficient of pressure is defined in Eq. (3), where ΔP is the pressure difference between the local and ambient pressure, A_{jet} is the area of the jet (1.188 in^2), and the T is the thrust of the jet. Coulliette and Plotkin offer an alternate definition in Eq. (4), for the coefficient of pressure for a zero thickness airfoil, where U_∞ is the free stream velocity, $u(x)$ is the horizontal velocity contribution, the h_{te} is the height of the trailing edge, and $h(x)$ is the height of the lower surface of the airfoil [13]. Traditional textbooks define the coefficient of pressure as depicted in Eq. (5), however, this form is not helpful for the current work since the dynamic pressure is dependent on the free stream velocity, which is absent from the model [14].

$$C_p = \frac{2(\Delta P)(A_{jet})}{T} \tag{3}$$

$$C_p(x) = 1 - \frac{u(x)^2}{U_\infty^2} = 1 - \frac{h_{te}^2}{h(x)^2} \tag{4}$$

$$C_p = \frac{p - p_\infty}{\frac{1}{2}\rho_\infty U_\infty^2} = \frac{p - p_\infty}{q_\infty} \tag{5}$$

The amount of pressure increase due to the presence of the ground, illustrated in FIGURE 5, is substantiated by an effort by a group of researchers at NASA Ames Research Center [15]. The group explored the forces and pressures induced on circular plates both in and out of ground effect. They found that there was an increase in the coefficient of pressure C_p while the plates were in ground effect. The group explored many height-to-plate diameter ratios, h/d_e , including 3.3 and 12.2. These two values represent the coefficient of pressure experienced as the plate is displaced further from the ground. As demonstrated by their effort, the closer the 20 inch plate was to the ground, the larger the coefficient of pressure. This fact is illustrated by simply looking at the scales of the coefficient of pressure in the detailed report. The scale for $h/d_e = 12.2$ is much smaller, indicating that the pressure is equally smaller.

While the NASA research effort illustrates the increase in the coefficient of pressure, the main advantage to ground effect is the increase in the coefficient of lift. Plotkin and Dodbele offer a definition of the alteration to the lift curve slope for a slender wing in ground effect in Eq. (6), where $C_{L\alpha}$ is the lift coefficient in ground effect, $(C_{L\alpha})_\infty$ is the lift coefficient out of ground effect, H is the height at the lowest point of the wing, and b is the wing span [16]. Eq. (6) culminates into FIGURE 6, which shows that at lower trailing edge height, the coefficient of lift in ground effect is substantially larger. The A in the graph is the aspect ratio of the slender wing. FIGURE 6 visually shows that the pressure experienced in ground effect results in a larger coefficient of lift, thereby demonstrating that a wing in ground effect has the potential to be enhanced when combined with the lift benefits of circulation control shown in FIGURE 3.

$$\frac{C_{L\alpha}}{(C_{L\alpha})_\infty} = 1 + \frac{1}{8}\left(\frac{b}{2H}\right)^2 - \frac{1}{32}\left(\frac{b}{2H}\right)^4 \tag{6}$$

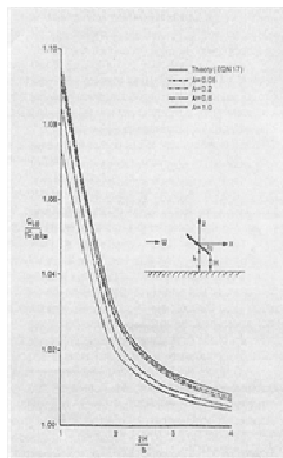


FIGURE 6 : Lift curve slope for slender wing in ground effect [16]

3 EXPERIMENT

3.1 Investigation

The investigation experimentally explores the impact that the radius of curvature, jet velocity and the height from the ground have on the delay in the flow separation of circulation control cylinders. The radius of curvature was changed between three different radii, including 0.520, 0.659, and 0.943 inches. The jet velocity was changed between three velocities relating to the volumetric flow rates of 10, 20 and 30 ft³/min. The height was changed six times. The heights are not constant values across all the radii, because the height in this effort is defined as the distance from the center of the cylinder to the top of the ground. Since the heights differ, when considering the height, the non-dimensional height-to-radius h/r quantity is used. Understanding the relationship between these three variables results in a better understanding of the effect circulation control and ground effect can have on each other.

3.2 MODEL, TEST SET-UP, TESTING METHOD

The setup for the testing of the three defined variables was conducted with the apparatus in FIGURE 7. This model is the same as the one used in the previous effort by the authors that defined the optimal radius of 0.659 inch and volumetric flow rate 30 ft³/min [5]. However, the model was reconfigured to have a variable ground for the current work. Similar to the original construction of the model, a computerized router table was used to cut out the peg holes on the side of the model; using a router table ensured that the holes were at the same locations on both the steel and LexanTM composite sides of the model, thereby ensuring the ground was level and parallel to the axis of the cylinder. The only other alteration to the original model was the plenum chamber. Previously, there was slight height variation in the height; the plenum was corrected so that the height as a function of the axial span was constant.

Along with the model, the components for obtaining the data needed to be assembled as are depicted in FIGURE 8. As visible in FIGURE 9, the instruments for data acquisition include a thermocouple, a pressure regulator, a volumetric flow rate sensor, and two shut-off valves. All of these devices were useful for the calculation of the jet velocity and the mass flow rate. While not visible in FIGURE 9, a pitot-static tube was employed to determine the actual velocity of the air leaving the slot. The principle sensor was the Heise digital pressure gauge. This measurement tool was used to measure the pressure from the surface pressure tap and the total and static pressure from the pitot-static tube.

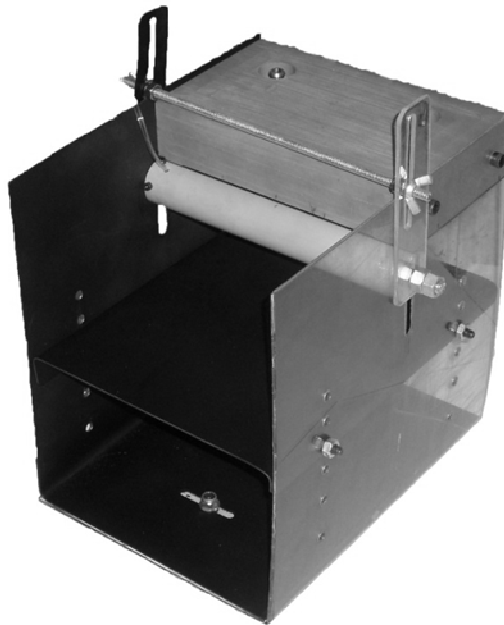


FIGURE 7: Model

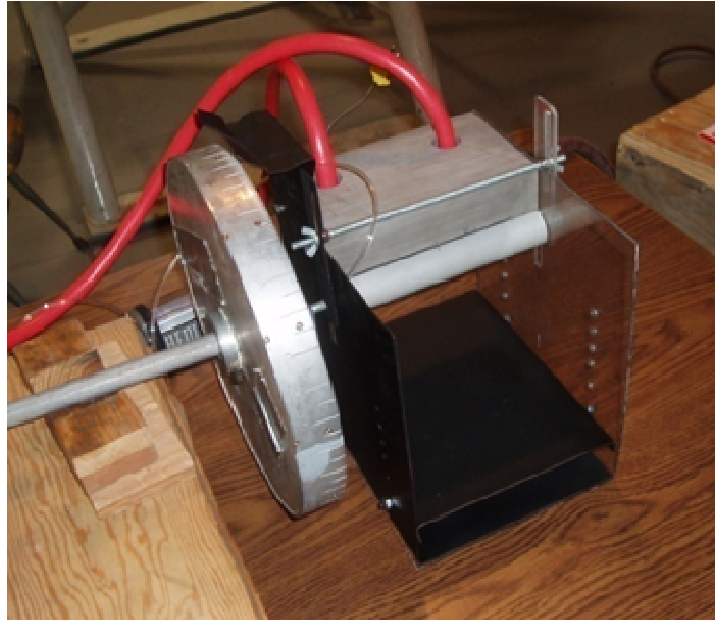


FIGURE 8 : Model with data acquisition equipment connected



FIGURE 9 : Data acquisition equipment

Over the course of completing the experiment, the same task was completed fifty-four times, for the six different heights, three different mass flow rates, and the three different radii. The repetitious task measured each surface pressure at every ten degrees, until the point of separation, where more points were measured to find a more refined separation location.

An important part of the testing method is to determine the location of the separation point. The point is generally located in step five of the test method and more accurately found in step seven. Upon reviewing the data, the separation point is defined as the point just before the ambient pressure is achieved. The separation point was chosen at the point just before the ambient pressure because if the pressure is the same as ambient the flow near the surface is no longer exposed to the vacuum, and thus free to detach

from the cylinder. FIGURE 14 shows the surface pressure of the cylinder with radius of 0.520 inch as a function of the angular displacement from the slot exit for the five different height locations measured. As the angular displacement increases, the surface pressure reached a horizontal, namely ambient pressure. The region of pressure lower than ambient pressure is the region where the jet is influenced by the surface, hence the Coanda effect is present and a vacuum is produced, thus holding the jet and entraining more air into the flow. Another measurement process was to determine the actual velocity of the jet. This value was obtained by measuring the static and total pressure of the airflow at five locations across the axial span of the slot, for the three different mass flow rates. Through Eq. (7) and Eq. (8), a variant of the continuity equation, the velocity of the jet could be determined.

$$P_{total} = \frac{\rho_j V_j^2}{2} + P_{static} \quad (7)$$

$$\rho_j = \frac{P_{static}}{T_j R} \quad (8)$$

4 RESULTS

4.1 Velocity Distribution

Across the span wise direction of the jet, the model exhibited a range of velocities, as shown in FIGURE 10. From this graph, it can be realized that there is a dip in the velocity from the left of the slot, labeled zero, to the center of the slot, indicated as location three. The explanation resulted from the use of structural bolts, which were placed in the plenum chamber to provide support for the plenum chamber and to ensure that the slot height remained constant. Since the bolts inhibited the flow of the air in the plenum, a lower velocity was produced, as measured at locations one through five. At both the zero and six locations, the velocities were expected to be lower than the maximum velocity, due to the interference of the side walls of the chamber on the flow. The maximum velocities of 184, 225, and 340 ft/s were determined, which correlates to the volumetric flow rates of 10, 20, and 30 ft³/min, respectively.

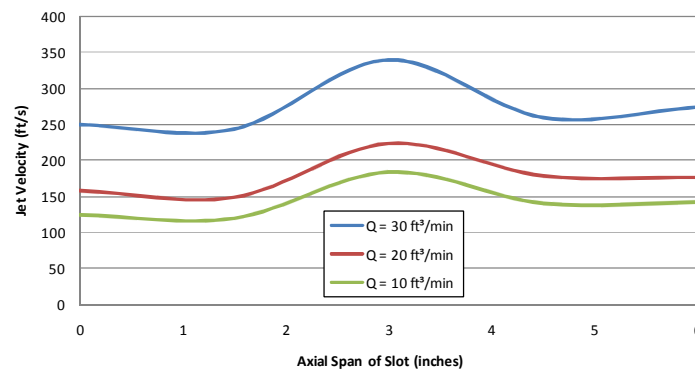


FIGURE 10 : Distribution of Jet Velocity

4.2 ANGLE OF SEPARATION AND GROUND HEIGHT

The first comparison of interest is the relationship of angular separation as a function of the height from the ground. As discussed, the h/r value is the variable of consideration when discussing the height from the ground. For FIGURE 11, FIGURE 12, and FIGURE 13, the same radius is compared for each respective graph which serves as a means to determine the impact that the volumetric flow rate has on the separation point, which is minimal. This indicates that a specific value for the rate is not the principal interest for initial analysis; similarly, if there is variability in a certain volumetric flow rate, such as the 20 ft³/min case in FIGURE 12 than that specific rate should be further investigated.

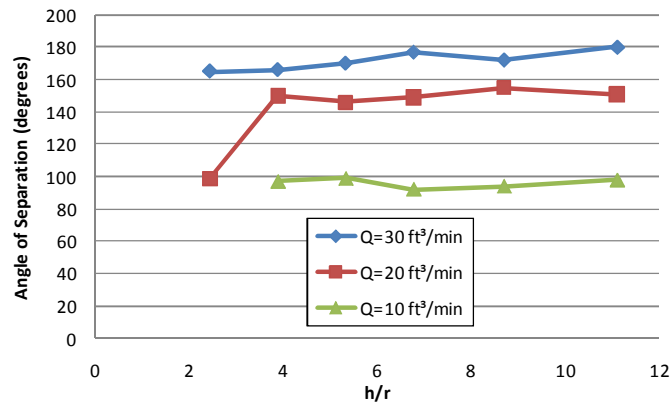


FIGURE 11 : Impact of ground proximity on the angular separation for r = 0.52 inch

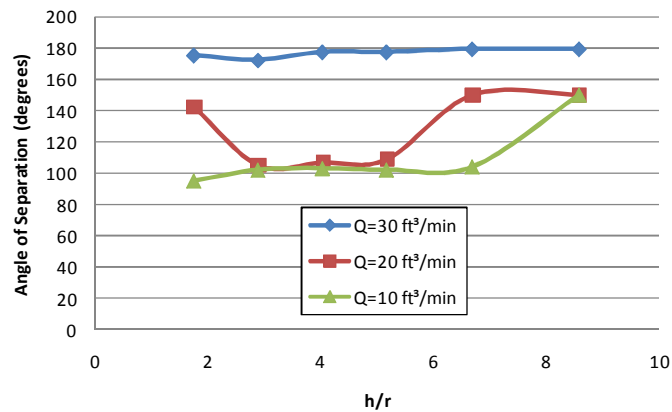


FIGURE 12 : Impact of ground proximity on the angular separation for r = 0.659 inch

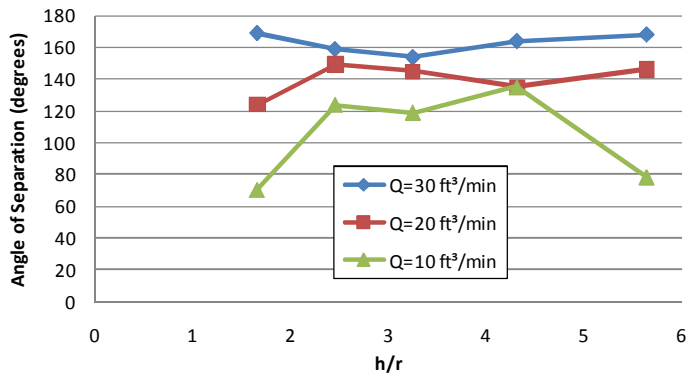


FIGURE 13 : Impact of ground proximity on the angular separation for r = 0.943 inch

When comparing the volumetric flow rate across the three different radii, each rate had a different degree of variability. For the volumetric flow rate of 30 ft³/min, the variability was relatively constant for the three radii. Most of the angles of separation for the subject volumetric flow rate were around 170 degrees. The relative constant angle of separation for 30 ft³/min indicates that this rate is not of further interest for this analysis. Since little change is occurring for the rate, it is safe to say that the angle of separation at 30 ft³/min is minimally affected by the variation in ground height. This conclusion is substantiated by the fact

that the subject rate is the fastest rate tested, suggesting that the faster the rate, the less it is impacted by the radii or height from the ground. Conversely, for the volumetric rate of 10 ft³/min, there were large variations between the three graphs and even within each graph, especially FIGURE 13. Thusly, 10 ft³/min is a rate for further analysis, since changes in the height alters the angle of separation in some manner. The final rate of 20 ft³/min did not exhibit the large disparity as 10 ft³/min, but it differs across each graph more than 30 ft³/min. However, since the lowest rate displays the largest change it will be the only volumetric rate for further analysis at this time. Future research will consider the relatively moderate variation in the 20 ft³/min volumetric flow rate and explore the pressure distribution just as is done for the lowest volumetric flow rate in the following section.

4.3 PRESSURE DISTRIBUTION

The next group of figures analyzes the surface pressure of the cylinder as a function of the angular displacement from the jet exit for the three radii, the different ground heights, and the subject volumetric flow rate. FIGURE 14, FIGURE 15, and FIGURE 16 all have a volumetric flow rate of 10 ft³/min, as discussed in the previous section. The figures culminate into FIGURE 17, which further illustrates the evident relationship of height to the pressure at an angle of 30 degrees in each the previous graphs (FIGURE 14, FIGURE 15, and FIGURE 16). The peak of all of these figures is a normalized pressure approaching unity, indicating that the recorded surface pressure is the same as ambient pressure, further illustrating that the flow separated from the cylindrical surface.

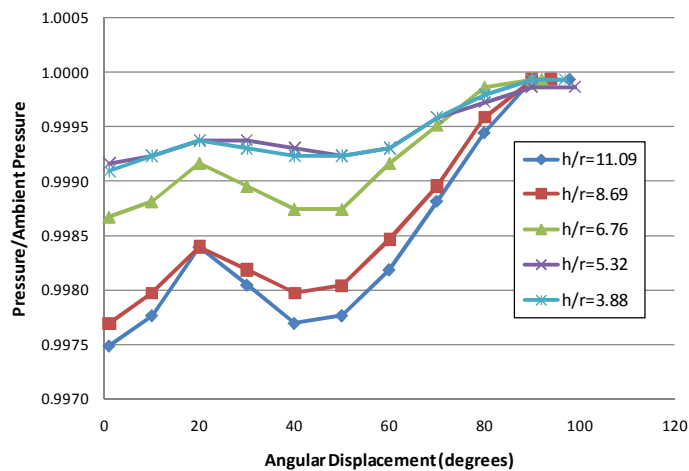


FIGURE 14 : Angular displacement vs. dimensionless pressure $r = 0.520$ inch

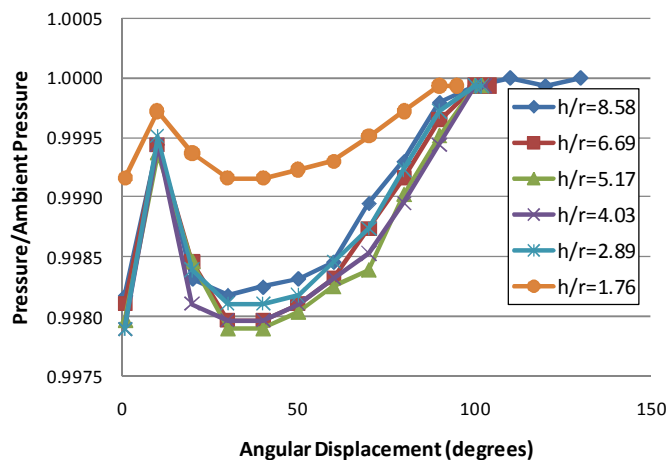


FIGURE 15 : Angular displacement vs. dimensionless pressure $r = 0.659$ inch

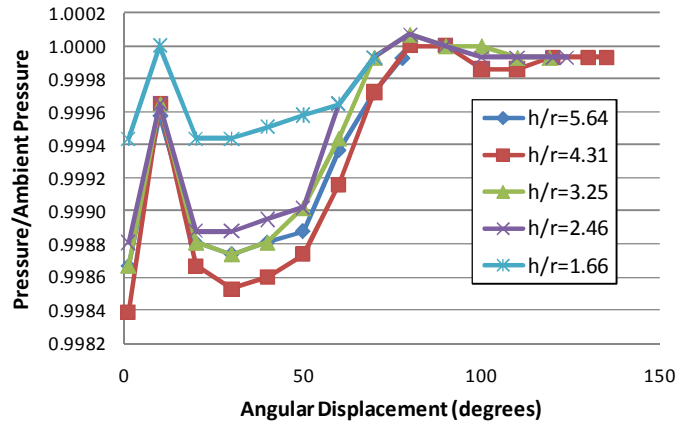


FIGURE 16 : Angular displacement vs. dimensionless pressure $r = 0.943$ inch

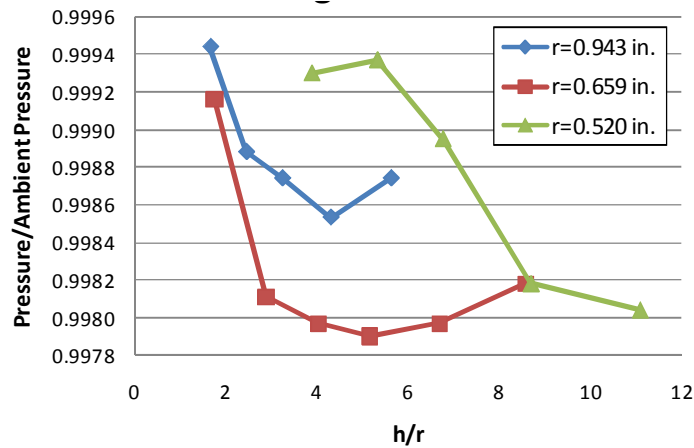


FIGURE 17 : Dimensionless pressure vs. h/r at 30 degrees from blown jet exit

FIGURE 14, FIGURE 15, and FIGURE 16 compare the angular displacement and the dimensionless pressure variable for each of the height from the surface tested. All of the figures have the same general trend, with a high pressure point (relative to ambient pressure) occurring in the 10 to 20 degree region. In one case, in FIGURE 16, for the h/r value of 1.66, the dimensionless pressure reaches one. It is suspected that this high pressure location is attributed to a weakening of the vacuum and a subsequent inflow of the high pressure airflow, characteristic of the entrainment Henri Coanda observed. Thus, in the subject region, more air is permitted to enter the vacuum further extending the angular displacement. Following the entrainment region, there is a significant drop in the pressure to another low pressure location at approximately 30 degrees for all of the radii. For a radius of 0.520 inch, in FIGURE 14, the low pressure region occurs later in the angular displacement than the other radii tested which indicates this value as a likely candidate for further research.

In addition, the results from FIGURE 14, as compared to the other two graphs, are spread out, such that the entrainment location and low pressure region occur at a larger angular displacement, suggesting that the smaller the radii, the larger the angular separation point. This conclusion is substantiated by previous work conducted by the authors, where, as the radii decreased, there was an increase in the angular separation point. However, in this previous study, the smallest radii, also 0.520 inch was not the optimal radii, illustrating that there is a threshold where a further decrease in the radii adversely impacted the separation location. While the initial test points of FIGURE 14 are prolonged, it is evident that the separation point occurs similar to the other radii. The final result of consideration from FIGURE 14 through FIGURE 16 is the separation location. Previous work suggested that the 0.659 inch was the

optimal radii in terms of largest angular separation point displacement. This effort also found that the 0.659 inch radii exhibited the largest average angular displacement when considering all of the height of the ground test locations. While the subject observation is not a new finding, its existence validates the test set-up of the current effort.

FIGURE 17 illustrates the dimensionless pressure vs. h/r at 30 degrees from the exit of the blown jet for each radius in FIGURE 14, FIGURE 15, and FIGURE 16. The location of 30 degrees for the blown slot exit plane was chosen based on the observation that the trough, or low pressure region, of each occurred approximately in this region. From the curve for the radius of 0.943 inch in FIGURE 17, it is evident that the pressure ratio decreases then increases, representing a minimum pressure point; the point of sign change correlates to an h/r value of 4.31. Similarly, for the curve representing 0.659 inch, the trend decreases and increases; the h/r value at the sign change is 5.17. Lastly, the h/r value for the curve illustrating the radius of 0.520 inch is 5.32, but the trend is reversed from the former two radii. The trend for the 0.520 inch radii increases and then decreases, representing a maximum pressure point. Furthermore, the two curves where the minimum is found represent the two highest radii, whereas the curve where the maximum point is found for the smallest radius. This finding indicates that there is a relationship between the radius of the cylinder and the ground height, and it appears that the preferred diameter is at some location between 0.520 and 0.659 inch diameters. Therefore there is an optimal h/r where circulation control and ground effect have the potential to enhance each other. In addition to the sign change finding, it is important to note that the h/r values at the sign change for the three radii, all occur at the relatively same value. This shows that there is a point where the ground maximizes or minimizes the surface pressure of the cylinder at 30 degrees. The unknown point resides between an h/r value of 4.31 and 5.32, which occurs at the largest radius and lowest radius tested, respectively. By identifying an optimal h/r value, it can further be stated that circulation control and ground effect, when combined, has the potential to enhance the lift augmentation of each other, since there is a relationship between the pressure and the h/r value.

The results from this current effort primarily serve as a preliminary investigation to determine whether there is enhancement from the amalgamation of ground effect and circulation control prior to the development of a technology demonstration model. As discussed from theoretical and empirical research, each of the two, separately, exploit phenomenon that yield proven benefits in terms of lift augmentation.. The current effort does not demonstrate an increase in the lift augmentation by combining the two technologies, as would be the goal in proving the discussed technology for implementation. Rather, the research enclosed serves as the first step in proving this methodology to increase lift but it does not serve as a reference to improve a known technology, especially since this technology is only recently being explored and as of yet to be installed in a commercial application. Results from this effort demonstrate that as geometric parameters were altered, general trends were formed, such as when the radii is increased there is a decrease in the localized pressure, and a subsequent low pressure region, resulting in further entrainment of air flow. However, in the previous trend conclusion, there is a threshold where a further increase in the radii, increases the localized pressure. The general trends such as the one discussed are the basis for continuing the development of a technology demonstrator, in the form of wind tunnel models. This next phase of experimentation will provide empirical data to delineate whether there is lift augmentation from the combination of the two technologies.

5 CONCLUSION

This effort concludes that there is a potential for the further enhancement of lift by combining the aerodynamics benefits of circulation control and ground effect. As shown from FIGURE 14 through FIGURE 17 there is an optimal h/r value, between 4.31 and 5.32, which is where the maximum and minimum for each radius resides. In addition to an optimal value, these figures demonstrate that at a radius between 0.520 and 0.659 inch, there is an inversion between a positive and negative function, respectively, showing that there is an optimal radius, as well as a height-to-radius relationship in regards to the surface pressure of the cylindrical surface.

For future work in this subject, there are a few areas for further investigation. The focus of the results section for this work was on only one volumetric flow rate of 10 ft³/min, since it demonstrated the largest variability. However, as shown in FIGURE 11 through FIGURE 13, the volumetric flow rate of 20 ft³/min

exhibited some degree of change, suggesting that there is a some sort of relationship between radius and the h/r value, as found in case of $10 \text{ ft}^3/\text{min}$.

Another area of work, which is currently being pursued by the authors, is using the findings from this effort in an environment of flow onset. The effort is amalgamating ground effect and circulation control by conducting wind tunnel experimentation and determining the lift enhancement.

6 ACKNOWLEDGEMENTS

This work was also made possible through the research funding from the West Virginia NASA Space Grant Consortium.

7 NOMENCLATURE

b	slot height
b	wing span, Eq. (6)
C_D	coefficient of drag
C_L	coefficient of lift
C_{La}	lift coefficient in ground effect
$(C_{La})_\infty$	lift coefficient out of ground effect
C_p	coefficient of pressure
C_μ	blowing coefficient
c	chord length
D	drag force
H	height at the wing trailing edge
$h(x)$	height of the lower surface of the airfoil
h_{te}	height of the trailing edge
h/d_e	height to plate diameter
h/r	ground height to radius of curvature
L	lift force
L/D	lift force/drag force
M_j	jet Mach number
\dot{m}	mass flow rate
P_∞	free stream pressure
P_o	plenum pressure
P_{static}	static pressure
P_{total}	total pressure
Q	volumetric flow rate
q_∞	dynamic pressure
R	universal gas constant, $1716 \text{ ft lb/slug } ^\circ\text{R}$
Re	Reynolds number
r	radius of curvature
t	slot height
T	thrust of the jet
T_j	temperature of jet
U_∞	free stream velocity
$u(x)$	horizontal velocity contribution
V_j, V_{jet}	velocity of jet

V_{∞}	free stream velocity
γ	ratio of specific heat
ΔP	local pressure difference
θ	angular displacement
ρ_j	density of the jet

8 REFERENCES

- [1] Byron W. Patterson et al., "Drag Reduction Methodologies for Circulation Control Applications".
- [2] Peter J. Mantle, *Air Cushion Craft Development*. Bethesda, MD: David W. Taylor Naval Ship Research and Development Center, January 1980.
- [3] Imantus Reba, "Applications of the Coanda Effect," *Scientific American* , pp. 84-92, 1966.
- [4] B.E. Newman, "The Deflexion of Plane Jets by Adjacent Boundaries - Coanda Effect," in *Boundary Layer and Flow Control Vol. 1.*: Pergamon Press, 1961, pp. 232-264.
- [5] Byron W. Patterson, Gerald M. Angle II, Emily D. Pertl, and James E. Smith, "Delay in Flow Separation for Circulation Controlled Cylinders," in *ASME International Mechanical Engineering Congress and Exposition (IMECE)*, Vancouver, British Columbia, Canada, November 12-18, 2010.
- [6] Robert J. McGhee and William D. Beasley, "Effects of Thickness on the Aerodynamic Characteristics of an Initial Low-Speed Family of Aviation for General Aviation Applications," Hampton, Virginia, June 1976.
- [7] Christopher M. Cagle and Gregory S. Jones, "A Wind Tunnel Model to Explore Unsteady Circulation Control for General Aviation Applications," in *22nd AIAA Aerodynamic Measurement Technology and Ground Testing Conference*, St. Louis, Missouri, 2002.
- [8] David T. Fisher, "Wind Tunnel Performance Comparative Test Results of a Circular Cylinder and 50% Ellipse Tailboom for Circulation Control Antitorque Applications," Monterey, California, MS Thesis 1994.
- [9] Jack P. Ambrosiani, "Analysis of a Circulation Controlled Elliptical Airfoil," West Virginia University, PhD Dissertation 1971.
- [10] Robert J. Englar, "Subsonic Two-Dimensional Wind Tunnel Investigation of the High Lift Capability of Circulation Control Wing Sections," Bethesda, Maryland, Report ASED-274 April 1975.
- [11] Harry J. Goett and W. Kenneth Bullivant, "Tests of N.A.C.A. 0009, 0012, and 0018 Airfoils in the Full-Scale Tunnel," Langley, VA, Report No. 647 1939.
- [12] Gerald M. Angle, "Data Tables from the Blue CC-NACA0018 Model Wind Tunnel Testing," Morgantown, West Virginia, 2009.
- [13] C. Coulliette and A. Plotkin, "Aerofoil ground effect revisited," *Aeronautical Journal*, pp. 65-74, February 1996.

- [14] John J. Bertin and Russell M. Cummings, *Aerodynamics for Engineers*, 5th ed. Upper Saddle River, NJ, United States of America: Pearson Prentice-Hall, 2009.
- [15] David C. Bellavia, Douglas A. Wardwell, Victor R. Corsiglia, and Richard E. Kuhn, "Forces and Pressures Induced on Circular Plates by a Single Lifting Jet in Ground Effect," Moffett Field, California, March 1991.
- [16] A. Plotkin and S.S. Dodbele, "Slender Wing in Ground Effect," *AIAA Journal Vol. 26 No.4*, pp. 493-494, April 1988.